Coordinated Frequency Regulation Using Solar Forecasting Based Virtual Inertia Control for Islanded Microgrids

Jiaming Chang, Yang Du, *Senior Member, IEEE*, Eng Gee Lim, *Senior Member, IEEE*, Huiqing Wen, *Senior Member, IEEE*, Xingshuo Li, *Member, IEEE*, and Lin Jiang, *Member, IEEE*

***Abstract*—Power system inertia helps the grid to maintain frequency stability. However, as photovoltaic (PV) generation continuously displaces synchronous generators (SGs) and reduces system inertia, it may result in system failure. Virtual inertia control (VIC) technology has drawn increasing attention because it enables PVs to increase system inertia by mimicking the characteristics of SGs. Energy sources are needed to implement the VIC strategy. Energy storage systems (ESS) can be used to provide such energy. However, the high-cost is still hindering its large-scale adoption. Although constant reserve power in PV has recently been proposed as an alternative for ESS, it can cause unnecessary power losses during the PV system working at a stable state. This paper proposes a forecasting-based VIC (FB-VIC) and coordinated reserve strategy. FB-VIC enables the PVs to serve as an alternative inertia supplier without using ESS. PV generation is pre-reserved based on the solar forecasting results, either at PV plant about to be shaded for local curtailment or other unshaded PV plants providing virtual inertia. The coordinated reserve strategy decides how much to reserve at the selected PV plant. It makes the system more robust to forecasting errors. The simulation results reveal that the proposed method can improve system inertia and suppress the frequency variation in a shorter time.**

***Keywords*—micro-grid, virtual synchronous generator, virtual inertial control, forecasting, coordinated reserve**

NOMENCLATURE

A. Acronyms

DG	Distributed generator
ESS	Energy storage system
FB-VIC	Forecasting-based virtual inertia control
GHI	Global horizontal irradiance
kNN	K-nearest neighbors
LSTM	Long-short term memory
MPP	Maximum power point
PV	Photovoltaic
RNN	Recurrent neural network
RoCoF	Rate of change of frequency
SG	Synchronous generator
SOC	State of charge
VIC	Virtual inertia control

B. Synchronous generator

D_s	Damping of SG
H_s	Inertia of SG
P_m	Power of SG
R	Ratio of SG power to frequency
t_a	Valve-actuator of SG
t_b	fuel system dynamics of SG
w_r	Actuator rotating speed
w_{ref}	Standard rotating speed

C. Photovoltaic

A	Area of PV panels
D	Virtual damping of PV
f	System frequency
F_{med}	Median point of forecasting
f_{ref}	Standard frequency
F_{sf}	Spot forecast power
G	Irradiance of PV
H	Virtual inertia of PV
K	Ratio of the nominal power to G&T
K_r	Ratio of VIC for coordinated reserve
L_{PV}	PV power uses for local curtailment
m	Forecasted shading PV stations
n	Total number of PV stations
P_c	Controlled power for VIC
P_r	Reserved power of PV
P_{mp}	Maximum power of PV
R_{PV}	Reserved power uses for FB-VIC
T	Temperature of PV

D. Energy storage system

$\$_{ESS}$	Generation cost of ESS
$\$_{FB-VIC}$	Generation cost of FB-VIC
η	ESS efficiency of the charge/discharge process
C_{ESS}	Extra investment costs of ESS
C_{PV}	Cost of PV
e_f	Proportion of the initial forecasting system
e_f	Proportion of the reserved power
e_r	Generation cost of FB-VIC

I. INTRODUCTION

PHOTOVOLTAICS (PV) generation has shown rapid growth to become one of the most promising renewable sources because of its clean, sustainable, and environmentally-friendly attributes [1]. Active distribution micro-grids are composed of local loads, the energy storage system (ESS), and distributed generators (DGs). The increasing penetration of PV in the DGs system promotes power structure changes in micro-grids. Frequency stability issues are one of the main problems in micro-grids [2], [3]. It is usually caused by the imbalance between load consumption and DGs. Generally, there are two ways to operate the micro-grid, namely, grid-connected mode and islanded mode. The grid-connected mode has a power

grid to exchange energy. The islanded mode cannot exchange energy with the power grid and is mainly adopted in remote area. For the grid-connected mode, the inappreciable power change in the local area enables supplementation by the grid system. For the islanded mode, high penetration of PV in DGs results in lower system inertia [4]. When system inertia is low, the generators may not raise power to regulate frequency promptly if the frequency drop occurs. In this situation, the characteristics of inertia and damping control provided by the synchronous generators (SGs) power are opposed to changes, which may result in system faults and disturbances [5].

Virtual inertia control (VIC) has recently been proposed to increase system inertia. One such example is a power system using VIC with the variable parameters for droop control is proposed in [6]. By simulating the characteristics of conventional SGs, the VIC technology can improve the system inertia response [7]. Moreover, the acceleration of the system is reduced and the deceleration effect is enhanced by changing the moment of inertia value. In [8], the study describes the development of small-signal models of VIC, and the details for mimicking the dynamic characteristics of SGs are realized.

Most of the VIC strategy requires extra energy from the ESS, such as batteries or super-capacitors [9], [10]. Although ESS is an effective way to provide sufficient VIC power, it leads to higher capital investment and operation costs. Furthermore, the additional SOC control increases energy loss when fully charged and elevates the control complexity [11].

Furthermore, adequate power supply for VIC can be maintained through PV power reserve control [12]–[14]. A method of using de-loaded PV to reduce power fluctuations was proposed a decade ago [15], [16]. In [16], an over-frequency case has been simulated, and the output saved 1.1 kW of power within 10 ms. Frequency regulation by PV has been achieved in a recent publication [17], [18]. Contemporary development in active power control [19]–[21] provides a solid foundation for these kinds of method. However, in order for sufficient power buffers to be provided to VIC when frequency deviation occurs, the above method usually requires constant power reduction, e.g. 10% of the maximum available power. Consequently, it causes continuous energy loss during operation times.

The ramp rate control using ultra-short-term forecasting or nowcasting to reserve power before shading arrives has been developed in recent years [22]–[28]. It has been reported in [29]–[31] that PV power ramp control can be realized without ESS using forecasting results, to reduce the photovoltaic power supply before the arrival of the cloud cover [32]. [33] proposed an ESS sizing method using short-term forecasting results, which can reduce the 50% ESS capacity needed to balance grid power. The above method typically requires accurate forecasting information on the PV power drop to reserve power at the local PV station, which is called local curtailment. However, the forecasting error is inevitable. PV cannot increase power to provide VIC if the forecast is inaccurate. A robust control method considering forecasting errors is needed.

The contribution of this paper is listed as follows:

1) A novel forecasting-based virtual inertia control (FB-VIC) is proposed to provide robust frequency control with considering forecasting error. When a large irradiance variation event is predicted for one of the PV plants, the other stable PV plants are controlled to reserve power. The power is released to provide energy for VIC to our best knowledge, this is the first work considering forecasting error.

2) A coordinated reserve method is proposed using probabilistic forecasting results and FB-VIC. It reduces the possible frequency fluctuation and improves the frequency control performance.

3) The frequency simulation has been built to evaluate and compare 4 types of control strategies. The critical point is obtained considering the spot forecast errors. When the forecast error is larger than the critical point, FB-VIC has been proved to have a better performance on frequency control.

The remainder of the paper is organized as follows. Section II introduces the proposed FB-VIC, and the coordinated reserve strategy is explained in Section III. Section IV then presents the simulation results of the method. Finally, we conclude the paper in Section V.

II. Proposed FB-VIC control strategy

Fig.1 shows the framework of the proposed FB-VIC control strategies in a micro-grid, including PV systems, load, and SG. There is a specific distance between PV stations. All PV stations have been divided into two groups: PV-A is defined as shaded PV stations, PV-B refers to stations with stable irradiance. When only PV-A is predicted to be shaded, PV-B begins to reserve power. The Total reserved power in PV-B is equal to the forecasted shaded power in PV-A. The reserved power is used as the source for VIC when there is a large frequency variation. Compared with the traditional local curtailment, the proposed strategy is improved the system's dynamic stability.

In [34], it has quantified the maximum effective geographical correlation distance between PV stations to be 10 km. [31] improved the forecasting control in terms of the ramp rate and the PV power. If the maximum ramp rate Rs is given, the detectable power fluctuation ΔPd can be found by

$$\Delta P_d = \frac{D_i}{V_i} \cdot P_m \cdot R_s \tag{1}$$

If the cloud shadow velocity is known as Vi, a longer distance between PV stations leads to higher power fluctuation. Thus, for the PV stations with a relatively large distance to each other, the power outputs are less likely to change together. The cloud shadow velocity and the distance between the target PV system determine when the system will be shaded. Considering the forecasting horizon is 1-min ahead, D_i/V_i needs larger than 1 minute.

When only PV-A is predicted to be shaded, PV-B begins to reserve power. The Total reserved power in PV-B is equal to the forecasted shaded power in PV-A. The reserved power is used as the source for VIC when there is a large frequency variation. In the case of the PV stations are close to each other, the smaller Di leads to a lower power fluctuation. PV-B cannot fully reserve the power because of the ramp rate limitation. A potential improvement is to reserve the required amount of power at different PV stations. The power is partially

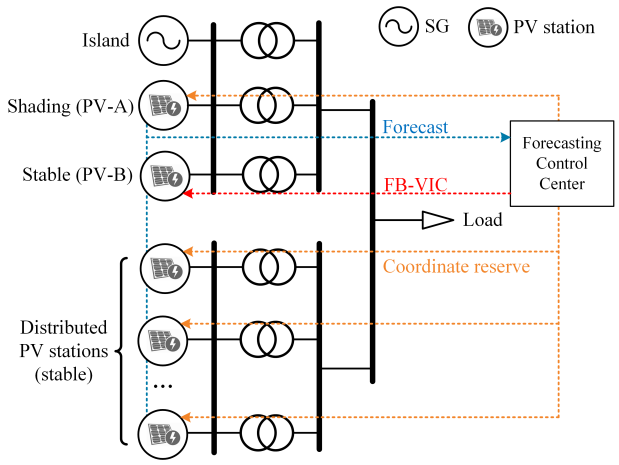

Fig. 1. Structures of the framework for FB-VIC strategies with forecasting.

reserved in PV-B when time permits and used for VIC. The rest of the power is coordinatively reserved in PV-A using local curtailment. This part of the control strategy is introduced in the coordinate control method. D_i is decreased when reducing of reserved power ΔP_d in PV-B for coordinate control, closer PV stations are allowed in the micro-grid system. The details of the proposed control strategy are provided in the following sections.

The details of the proposed control strategy are provided in the following sections.

A. Control of SG

The SG module is created within MATLAB/Simulink as a p.u. (per unit) structure. PI controllers and actuators are used for power control. SG torque is adjusted by changing the fuel's value, as shown in Fig.2. The SG output power changes with the frequency deviations. It may be caused by PV power or load demand change in the slip range. The main block diagram of the speed governor model includes the valve-actuator and the fuel system dynamics is described in [35]. The power response of the SG in the dynamics system is determined by

$$P_m = w_r \cdot (w_{ref} - w_r) \cdot \frac{K \cdot G_{PI}}{(t_a s + 1) \cdot (t_b s + 1)} \tag{2}$$

where ω_r is the actuator rotating speed, ω_{ref} is the standard rotating speed, K is the gain, G_{PI} is the PI controller, R is the ratio of power to frequency, t_a is the valve actuator, and t_b is the fuel flow. The parameterize value of ta is 0.332 and tb is 0.212, which makes the simulated active power matches the measured value. A new standard module is presented in Fig.3 to simplify the power to frequency relationship and the use of inertia and damping factor instead of the valve characteristics in SG. The SG output power simplified as

$$D_p \cdot \Delta\omega = (2H_s s + D_s) \cdot P_m \tag{3}$$

where H_s is the SG inertia, D_s is the SG damping factor and D_p is the droop coefficient.

B. MPPT control of PVs

A single-stage PV model is explained in [36], [37] estimates the maximum power points (MPP) for PV power sources. For equation (4), it is observed that the PV power is mainly affected by irradiance and temperature. The irradiance is proportional to power, and temperature is inversely proportional to power. Using 25°C as the nominal standard, the MPP estimation method expression is represented by

$$P_{mp} = \frac{25\mathrm{C} \cdot G}{T} \cdot \frac{K}{\frac{\sqrt{A}}{2\pi \cdot 0.02} s + 1} \tag{4}$$

where G is the instantaneous irradiance panels, T is the PV station temperature, K is a constant parameter, and A is the PV panel area. The complexity of the second-order polynomial fitting in the conventional PV model is reduced, and the MPP tracking speed is guaranteed by using (3). When the MPP of a PV panel is determined by P_{MP}, it is convenient to change the PV power from point A to B. The voltage signal V_{cmd} is used to operate the working point to the inverter, displayed in Fig.4. The P_{MP} characterizes the maximum available power and the P_{SET} determines the reserve power by changing the working point.

C. Short-term forecasting

A preliminary experiment on forecasting solar irradiance using a naive Long-Short Term Memory (LSTM) model is presented. The module can handle long-term time dependencies and cope with exploding and vanishing gradients utilizing a standard recurrent neural network (RNN). LSTM is a variation of RNN architecture used in deep learning. A hybrid framework integrated by deep learning is proposed in [38] to predict short-term PV power in the form of a time series. A short-term PV power forecast model based on the extremum learning machine is proposed in [39].

The model is trained on a publicly available dataset obtained at Folsom, CA. The dataset provides 1-min temporal resolution data, including irradiance values and sky images, and secondary data such as satellite imagery, meteorological data, and features extracted from these data over three years

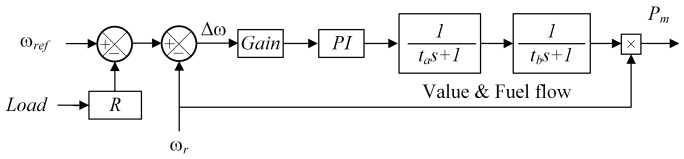

Fig. 2. Block diagram of the SG control module.

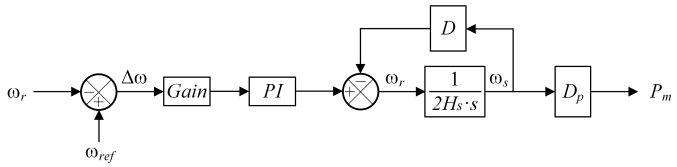

Fig. 3. Block diagram of the simplified SG module to VIC control.

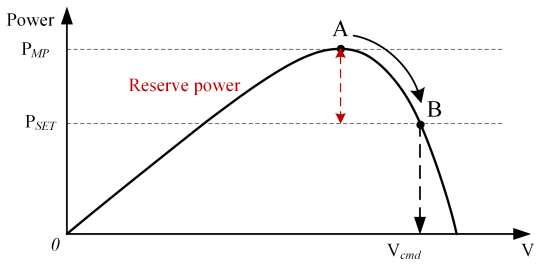

Fig. 4. Principle of PV power reserves, with the movement of the operating point away from MPP.

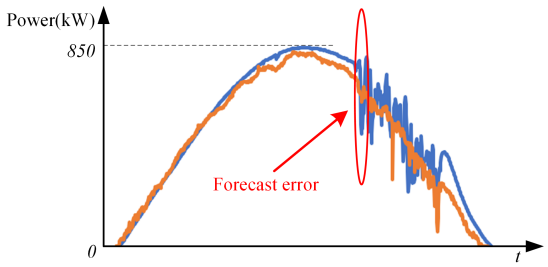

Fig. 5. Single-day spot forecasting results.

(2014-2016). For more details of the dataset, please refer to the original paper [40]. In this work, only global horizontal irradiance (GHI) is used as the input for the LSTM model.

Single-day spot forecasting results from the test set are displayed in Fig.5. The forecast has large errors compared with the target power values over time. Different error levels are used in this work to discuss their effect on frequency performance. The probabilistic forecast results of the forecast error points in Fig.5 using k-nearest neighbors (kNN) is demonstrated in Fig.6, the higher bar chart has more probability for different forecasted power. There is a difference between the median power and maximum probability power (almost spot forecast point).

D. Forecasting based VIC

Fig.7 illustrates the FB-VIC control strategy using 1-min future irradiance data consistently in the cloud control block. The PV system worked at MPPs when steady-state of irradiance was forecasted. However, when the forecast result changes, a reserved signal P_r is sent to the cloud controller, then a command signal V_{cmd} is used to reserve power in the FB-VIC controller is sent. In this case, a PID controller

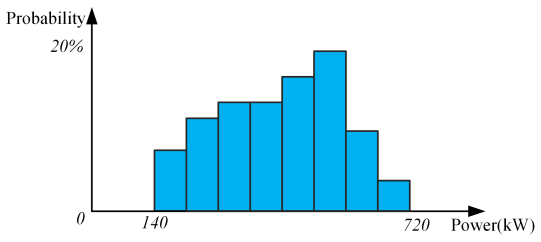

Fig. 6. Probabilistic forecasting outcomes at point of irradiance variation.

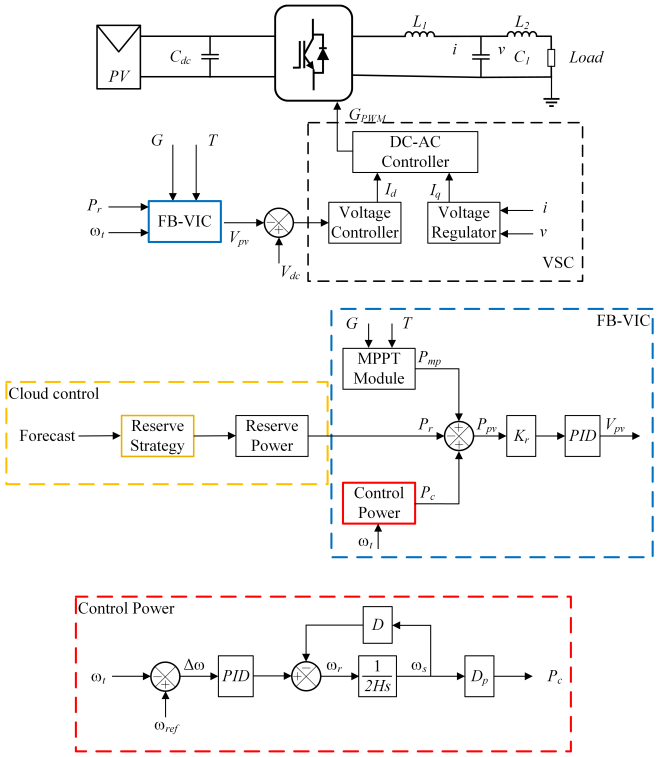

Fig. 7. Control strategy of the proposed FB-VIC.

provides improved frequency regulation. The voltage and current from the AC side represent the reference. Then, the voltage and current regulator is used to generate the PWM signal by DC/AC converter control. The PV power is reserved by changing the working point, which is represented as the following rule

$$P_{MP} - P_r = P_{SET} \tag{5}$$

where P_{MP} is the maximum power estimate, P_r is the reserved power estimated by control, and P_{SET} is the working point after power reserve. It has a ramp controller in P_r to ensure frequency stability during power reserve. The ratio of the ramp controller is limited by forecasting information. Details are elaborated in the next section.

PV can provide inertia after power reserve control. When the frequency changes, the PV starts to inject power into the system. In this case, the transient PV power P_{pv} is determined by

$$P_{pv} = P_{SET} + P_c \tag{6}$$

where P_r is the reserved power, and P_c is the controlled power for VIC. The available power of P_c is limited by P_r. It using the $p-w$ droop coefficient D_p for the FB-VIC method to allow the VIC to operate at the required frequency level. Then, it converts frequency change to power regulation. Virtual inertia H and damping D are set as SG characteristics. PV and SG have the same performance as inertia control. The control function is determined by

$$D_p \cdot \Delta\omega = (2Hs + D) \cdot P_c \tag{7}$$

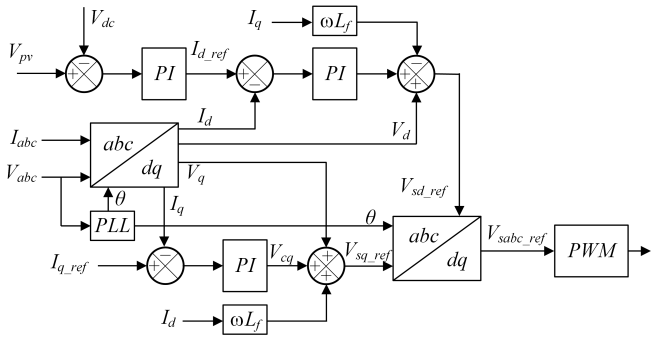

Fig. 8. VSC control diagram.

Fig.8 shows the VSC (voltage source converter) control diagram. A feedback linearization scheme with feedforward PV current signal is adopted from [41]. The PWM (Pulse Width Modulation) signals can be generated by current and voltage at the AC side.

III. Reserve Strategy

We have two PV power reserve options: FB local curtailment, and FB-VIC reserve. FB local curtailment means using forecasting information to reserve power in the local PV station before shading arrives. FB-VIC reserve is using forecast information to reserve power in geographically separated stabled PV stations instead of shaded PV stations. The reserved power is released for frequency control providing virtual inertia. Section A discusses frequency control performance under different levels of spot forecasting errors. Section B proposes a coordinated reserve strategy based on the probabilistic forecasting results.

A. Frequency control considering spot forecasting error

Spot forecasting frequently involves errors. The local curtailment and FB-VIC methods have varying performances for separate forecasting errors. The RoCoF is used as a control trigger to discharge the reserved power. The VIC starts to work at RoCoF out of limitation. Small frequency variations in the reserve strategy do not affect the PVs; they can avoid VIC during reserve power. According to Eqs. (2) and (6), if the inertia and damping of SG have the same PV and SG values, then the PV exhibits similar frequency control performance. As shown in Fig.9, the blue line is the actual power change, and the reserve power is equal to the forecasted power drop when the forecast error is large enough. Local reserve power can only provide for half of the required power. The power deficit causes frequency variation, and frequency regulation only relies on SG. For the FB-VIC control strategy, with the same reserved power from other unshaded PV stations, double virtual inertia can be provided to make up for total power requirements instead of directly compensating for the power drop. Thus, local curtailment and FB-VIC have the same performance. Simulations have been carried out to compare the frequency regulation performance of MPPT and local curtailment strategies under different forecasting error levels. The findings confirm that FB-VIC performs better when the

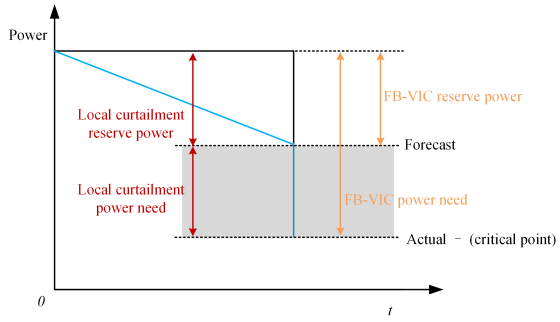

Fig. 9. Critical point of local curtailment and FB-VIC in the spot forecasting error.

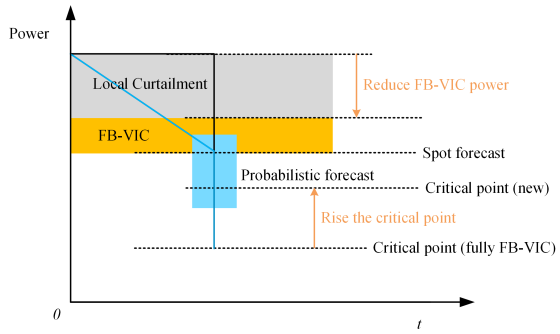

Fig. 10. Critical point of local curtailment and FB-VIC in probabilistic forecasting.

error is larger than a specific value (critical point). Otherwise, local curtailment is the better solution. More details about the simulation results are reported in the next section.

B. Coordinated reserve strategy using probabilistic forecasting

It is apparent from the previous section that the optimal solution for selecting where to reserve depends on the forecasting predictions. Given that there are errors in all the forecasting methods, a probabilistic forecasting method is needed. Compared with spot forecasting, probabilistic forecasting results provide a predictive probability distribution for

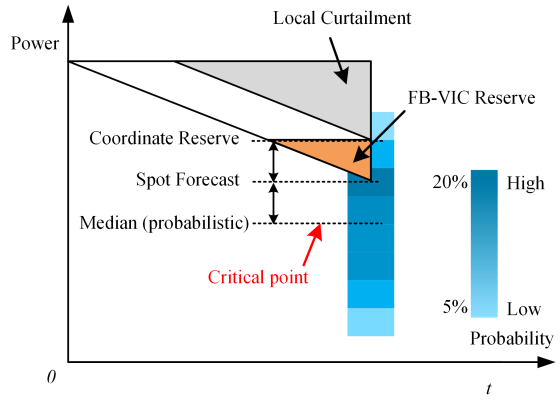

Fig. 11. Power reserve strategy with coordinated control and probabilistic forecasting.

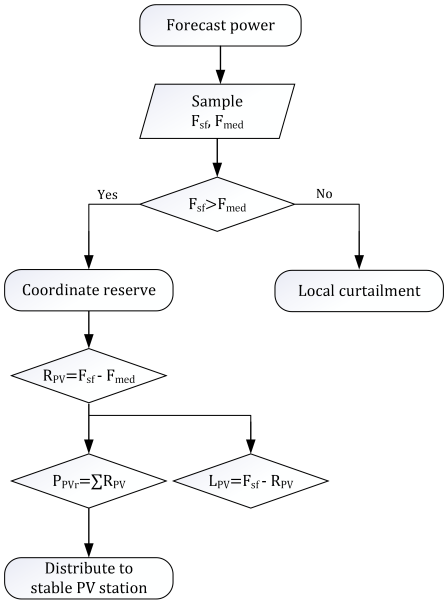

Fig. 12. Flowchart of the proposed coordinated reserve strategy.

a range of irradiance. In Fig.10 the blue region is all the possible forecasted irradiance; the critical point falls under this region, which means optimal control can never be achieved if we only use the local reserve or FB-VIC reserve techniques. A hybrid method is mandatory. The critical point can be moved by reserving power from both reserve methods. According to the above section's conclusion, by reducing the reserve from FB-VIC to only the yellow region, the critical point is lifted. The coordinated control strategy can freely set the critical point by changing the ratio between the local reserve and the FB-VIC reserve. We chose the median of the probabilistic forecasting output to be the critical point. There is limited power to provide adequate inertia. If the critical point is too close to the spot forecasting result, it is more likely to have better performance in the probability of frequency deviation but lower frequency nadir. In contrast, if the critical point is too far away from the spot forecasting result, the coordinated control has extensive frequency deviation but higher frequency nadir. As shown in Fig.11, coordinated control allocates the required reserved power to local reserve and FB-VIC reserve separately. The darker the color is, the higher the possibility. We set the median of the probabilistic forecast as the critical point. The point can be separately determined through spot forecasting. FB-VIC reserve power (orange part) is equal to the difference between the spot forecast point and the probabilistic forecast median. The coordinated control strategy is shown in Fig.12, F_{med} is the median of probabilistic forecasted power, and F_{sf} is the spot forecasting power. If F_{med} is less than the F_{sf}, the coordinated reserve is used. FB-VIC reserved power R_{PV} is the difference between F_{mid} and F_{sf}. The local curtailment power L_{PV} is equal to F_{sf} minus R_{PV}. P_{PV_r} is the total FB-VIC satisfactory power to be reserved in stable PV stations. We can extend this coordinated reserve strategy to handle more than two PV stations. The required reserve power is evenly distributed to other PV stations without forecasted shading. This distribution can be represented by

$$\Delta P_{pv_1} + \Delta P_{pv_2} + \Delta P_{pv_3} + ... = \Delta P_{SG} \tag{8}$$

where ΔP_{pv} is the forecasted PV power change in frequency regulation, and ΔP_{SG} is the SG power change in frequency regulation. Distributed PV stations can then be considered as one, and we can evenly spread inertia with SG. The shading is asynchronous in a distributed PV system that has maintained the distance among the PV stations. Thus, the forecast reserve power can be distributed to stable PV stations. Power reserve to deal with unpredictable disturbances, the ratio of VIC for the constant reserve station and coordinated reserve stations can be found by

$$K_r = \frac{\Delta P_{PV_r} - L_{PV}}{n - m} \tag{9}$$

where K_r is the ratio of VIC for coordinated reserve in each station, n is the total number of PV stations, and m is the forecast shading PV station. In this coordinated reserve strategy, virtual inertia power is dispersed to the stable PV station and quickly provides VIC to regulate frequency in PV power reduction occurrences.

IV. Simulation Results

An islanded microgrid has been modeled using MATLAB/Simulink. The single line diagram of the modeling is shown in Fig.1. The FB-VIC strategy using 2 PV stations to simulate the effect of the spot forecasting errors on frequency variation. One of the PV stations will be shaded according to the forecasting results, the other one has stable irradiance. The coordinate control strategy redistributes the required reserve power to local shading PV stations and remote stable PV stations. The corresponding parameters of the tested system are given in Table I.

The sudden output power change in PV1 is modeled as follows. The initial PV power output is 466 kW, then it suddenly decreases to 90 kW at 58 s, and the forecast power at 58 s is 290 kW, which has a 200 kW forecast error. PV2 receives constant irradiance at the same time, which is equivalent to 724 kW.

To validate the effectiveness of the proposed FB-VIC strategy, simulations have been carried out as shown in Fig.7. Traditional control strategy using the typical MPPT algorithms such as the fixed-step-size perturb and observe (P&O), which is introduced in [42]. PV always works at MPP makes it cannot contribute to frequency control since no additional power can be used to compensate for the power loss. The local curtailment method uses PV active power control, which has explained in [30]. Fig.13 shows the implementation of the local curtailment. For the ramp down control, the power of PV can be curtailment before the actual shading arrives. The ramp rate is controlled by the Rs, then the power ramp can be directly smoothed and cause no effect when shading arrives. It is called local curtailment. An ESS control strategy in the frequency containment reserve (FCR) market has been proposed in [43]. State of Charge (SOC) is controlled according to the frequency

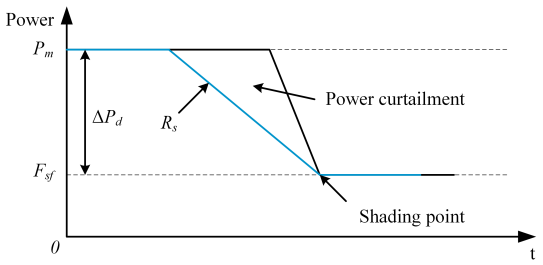

Fig. 13. PV active power control of local curtailment.

deviations. MPPT, ESS, and local curtailment methods are simulated, the results have been compared with the proposed FB-VIC strategy.

TABLE I
THE CORRESPONDING PARAMETERS OF THE TESTED SYSTEM

Parameters	Value
Constant inertia of SG Hs	0.6s
Constant damping of SG Ds	1.2 p.u.
Virtual inertia of PV H	0.6s
Virtual damping of PV D	1.2 p.u.
Capacity of SG	2MW
Capacity of shading PV	480kW
Capacity of stable PV	724kW
Load	1.3MW
Ramp rate Rs	4 W/s

A. Traditional MPPT control

For the traditional MPPT control method, PV power has to operate at MPP all the time. At 58 s, the forecasted PV1 station drop from 466 kW to 90 kW with 200 kW forecasting error is displayed in Fig.14(c). The SG begins to provide extra power only after 58 s, as presented in Fig.14(g). According to Fig.14(a), the islanded microgrid system has a stable frequency at 50 Hz before PV shading. After 58 s, the frequency nadir reduces to 49.56 Hz. As illustrated by the blue line in Fig.14(b), the traditional MPPT control method takes 1.6 s to balance the frequency at 50 Hz. PV systems always operate at MPPs. It can be seen as the blue line in Fig.14(d),14(f). For SG, it has 0.085 p.u. before 58 s. When the PV1 is shaded, the power reduces to 90 kW within 58 s. Surplus power compensates for the PV power loss. The blue line demonstrates the SG power changes in Fig.14(h).

B. Local active power curtailment

Frequency control using local active power curtailment strategy is evaluated. Fig.14(c) displays the maximum available power of PV1 as 466 kW. The PV1 works away from the MPPs with ramp control to operate with frequency deviation. It reserves 172 kW, which is equal to the forecast results. After 58 s, the PV regulates the frequency for the reserved power. Due to the forecasting error (200 kW), the PV system works at MPP (90 kW), which is lower than the operation point. There is no room for this PV station to provide extra power. After 1.5 s, the system frequency is regulated back to 50 Hz. The frequency is regulated only by employing SG. During the

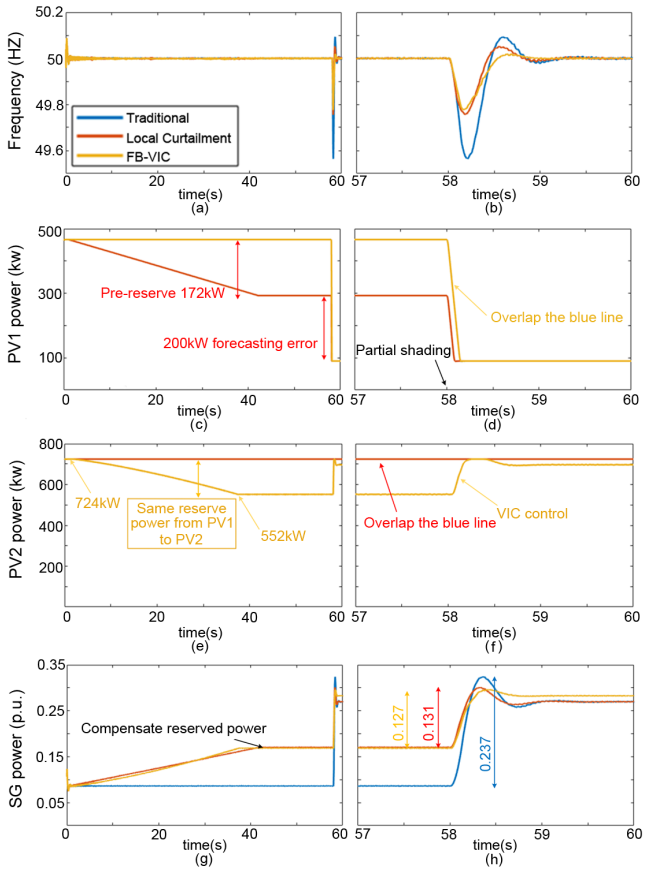

Fig. 14. Comparison of three strategies. (a) frequency response, (b) close-up view of the frequency response at the point of PV power variation, (c) partial shading PV station (PV1) output power, (d) close-up view of the PV output at the point of PV power variation, (e) no partial shading PV station (PV2) output power, (f) close-up view of the PV output at the point of PV power variation, (g) SG output power, (h) close-up view of the SG output at the point of PV power variation

local curtailment strategy, SG injects an extra 0.131 p.u. power during the PV power drop shown in Fig.14(h).

C. FB-VIC

The FB-VIC strategy uses 1-min future power forecasting data. During VIC operations, if a PV power decrease has been predicted at one of the PV stations (PV1), the reserve power of other PV station (PV2) is used to provide VIC. Compared with the local active power curtailment control strategy, both have the same reserved power, but FB-VIC uses PV2 to reserve power. Before 58 s, PVs are operated at MPP, as shown in Fig.14(e). When the power of PV1 is forecasted to decrease, then the PV2 power is pre-reserved before PV1 is shaded. For this moment, PV2 has moved the working point away from 725 kW to 552 kW (172kW, same as section B). It can be seen from Fig.14(g) that the SG output power increases from 0.087 p.u. to 0.169 p.u. to regulate the frequency at a stable value of 50 Hz. After 58 s, PV1 decreases to 90 kW, and the PV2 has power reserved for VIC to regulate the frequency. According to Fig.14(h), inertia control for SG provides power from 0.168 p.u. to 0.295 p.u. for frequency regulation. Comparing these methods, FB-VIC

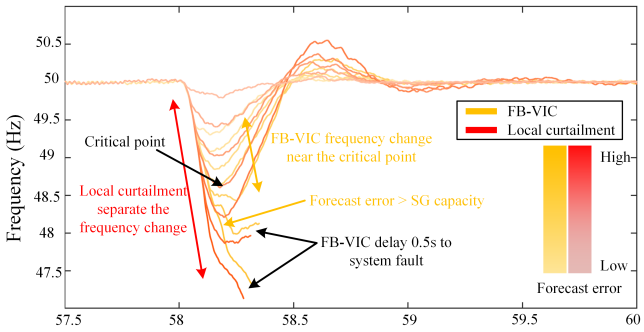

Fig. 15. Frequency response of high PV penetration.

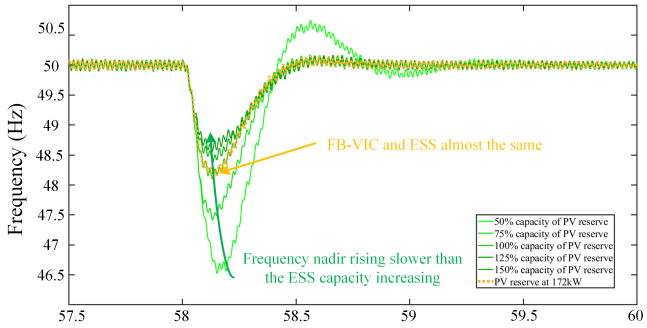

Fig. 16. Frequency deviations in different levels ESS capacity.

has reduced 46.4% and 3% SG instantaneous capacity. There is 0.237 p.u. additional SG power for inertia control in the conventional MPPT method, and 0.131 p.u. extra SG power for the local curtailment methods. The frequency deviation can be limited to a smaller range by the proposed FB-VIC method with shading. Furthermore, it only uses 0.88 s to restore the frequency, as presented in Fig.14(b).

Fig. 15 shows the frequency response for the system with a higher level of PV penetration. The PV power ratio is increasing to 75% of the total power. The SG capacity is reduced to 400kW. Frequency deviations happened and near the critical point by using the FB-VIC strategy. The local curtailment strategy is more sensitive to forecast error. The frequency fluctuates between 48Hz and 50Hz. When the forecast error is larger than the available power of SG, the frequency cannot come back to 50Hz, then the system fault. Moreover, FB-VIC delay 0.5s to the system fault. The smaller SG capacity also results in fluctuations and distortions in the system frequency regulation. As a result, the smallest required SG capacity needs to be larger than the maximum possible forecast error.

D. ESS

When we design the ESS capacity is the same as the power reserved by FB-VIC, our proposal and ESS method have the same performance. As shown in Fig.16, the orange dashed line is the frequency response of FB-VIC, the green lines show ESS control with different capacity levels. Larger ESS capacity leads to higher frequency nadir. However, the frequency response improved less with ESS capacity higher than 100% PV reserve, this is because the exceeding ESS power is not fully used for frequency regulation.

The cost of PV generated power C_{PV} is estimated to be 0.045 \$/kWh which is in line with the values considered in [44]. Due to the lifetime of the PV plant is 20 years, and ESS needs to be replaced after its 10 years lifetime, with an estimated second 10 years at 60% of the original price [45]. The generation cost of ESS can be given by

$$\$_{ESS} = \frac{1.6C_{ESS}}{\eta} + C_{PV} \tag{10}$$

As the ESS size is equal to reserved power in the PV station, extra investment costs of ESS C_{ESS} can be calculated assuming a price of 0.003 \$/kWh and ESS efficiency of the charge/discharge process η is 92% [45]. Thus, the ESS control strategy has cost 0.0502 \$/kWh. FB-VIC losses power caused by power reserve. The generation cost is calculated as

$$\$_{FB-VIC} = C_{PV} \cdot (1 + e_f + e_r) \tag{11}$$

e_f is the proportion of the initial forecasting system, it is 0.5% as used in [44]. e_r is the proportion of the reserved power, it is 8% based on former case studies [46]. Therefore, the FB-VIC has cost 0.0488 \$/kWh. The FB-VIC has reduced the ESS cost and smoothed the frequency similar to the ESS control strategy with the same capacity.

E. FB-VIC critical point

Simulations have been carried out to analyze the frequency control performance under varying error levels for both local curtailment and FB-VIC. The proposed scenario has a 172 kW power drop at PV1 predicted by spot forecasting. The same amount of power is reserved at PV1 for local curtailment and PV2 for FB-VIC. Fig.17 illustrates the findings when the forecasting error is 172 kW, which is equivalent to the reserved power. Consequently, the two methods have very similar performance regardless of the size of the PV plants.

Table II displays the simulation outcomes for different forecasting error levels. When the forecasting error is smaller than the reserved power, local curtailment is the superior solution. Otherwise, when there is extensive error, FB-VIC should be used. We call it the ”critical point” when the forecasting error equals the reserved power. Thus, Section III(A) ’s critical point method can be proved and used for the coordinated control strategy.

TABLE II
FREQUENCY NADIR IN DIFFERENT FORECASTING ERROR

Forecasting error (kW)	Frequency nadir (Hz)	
	FB-VIC reserve	Local curtailment
112	49.86	49.81
142	49.81	49.79
172	49.78	49.78
202	49.74	49.77
232	49.72	49.76

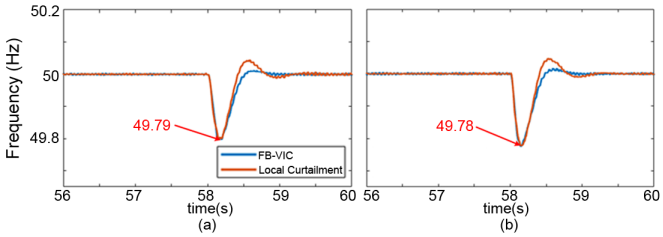

Fig. 17. Frequency control performance of local curtailment and FB-VIC when the forecasting error equals the reserved power (a) small PV power plant, rated power 466kW, b) large PV plant, rated power 724kW

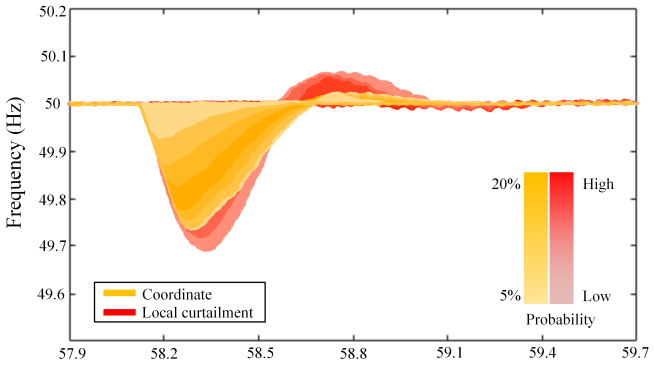

Fig. 18. Frequency with coordinated control and local curtailment with probabilistic forecast information.

F. Coordinated reserve control

Coordinated reserve control is proposed to share the required reserve power between group A (directly before the onset of shading) and group B (normal operation) PV stations using probabilistic forecasting results considering the spot forecasting error. A simulation model has been developed to demonstrate the performance of the suggested coordinated reserve method. Six PV stations have been modeled, and 2 of them are directly before the onset of shading (group A). Within the 4 PV stations under normal operation, 1 PV station operates at 10% constant reserve mode, and the other 3 stations are ready to reserve power according to the command from the control center. We assume Fig.6 represents the forecasting result. For example, there is a 3.98% chance the power decreases to 647.5 ˜ 720 kW. The frequency response is simulated and plotted in Fig.18 with the lightest color using both the coordinated method (yellow) and local curtailment (red). The simulation is repeated several times for each forecasted power. The resulting frequency response is highlighted with the associated probability, with the darker color representing higher probability. Table III shows that the frequency nadir and peak have been regulated in a smaller range using the coordinated reserve method, and it takes less time to stabilize the frequency. Overall, the proposed coordinated method overperforms the local curtailment method.

V. Conclusion

This paper proposes a FB-VIC method to control frequency variation caused by shaded PV stations without expensive ESS. Based on the forecasting results, power is reserved to provide energy for virtual inertia control. Spot forecasting is always associated with errors. FB-VIC has better performance when larger forecasting errors exist. In contrast, local curtailment is an enhanced solution for smaller errors. The critical point is identified to separate these two cases. A coordinated reserve strategy is recommended to find the optimal solution using probabilistic forecasting results. Simulation results are then presented to demonstrate the effectiveness of the proposed method.

TABLE III
Frequency deviation of coordinated control and local curtailment

	Coordinated control	Local curtailment
Lowest frequency nadir	49.73 Hz	49.68 Hz
Highest frequency overshoot	50.02 Hz	50.07 Hz
Settling time	0.9 s	1.5 s

References

[1] M. Woodhouse, R. Jones-Albertus, D. Feldman, R. Fu, K. Horowitz, D. Chung, D. Jordan, and S. Kurtz, "On the path to sunshot: The role of advancements in solar photovoltaic efficiency, reliability, and costs," National Renewable Energy Laboratory (NREL), Tech. Rep., 2016.

[2] M. Dreidy, H. Mokhlis, and S. Mekhilef, "Inertia response and frequency control technologies for renewable energy sources," *Renewable and Sustainable Energy Reviews*, vol. 69, pp. 144–145, 2017.

[3] A. Narendra, N. V. Naik], A. K. Panda, and N. Tiwary, "A comprehensive review of pv driven electrical motors," *Solar Energy*, vol. 195, pp. 278 – 303, 2020.

[4] F. Blaabjerg, R. Teodorescu, M. Liserre, and A. V. Timbus, "Overview of Control and Grid Synchronization for Distributed Power Generation Systems," *IEEE Transactions on Industrial Electronics*, vol. 53, no. 5, pp. 1398–1409, 2006.

[5] H. Bevrani, M. Feizi, and S. Ataee, "Robust frequency control in an islanded microgrid: Hinf and μ-synthesis approaches," *IEEE Transactions on Smart Grid*, vol. 7, pp. 706–717, 2015.

[6] J. Alipoor, Y. Miura, and W. Fan, "Power system stabilization using virtual synchronous generator with alternating moment of inertia," *IEEE Journal of Emerging and Selected Topics in Power Electronics*, vol. 3, pp. 451–458, 2015.

[7] H. Bevrani, T. Ise, and Y. Miura, "Virtual synchronous generators: A survey and new perspectives," *Electrical Power and Energy Systems*, vol. 54, pp. 244–254, 2014.

[8] J. Liu, Y. Miura, and T.Ise, "Comparison of dynamic characteristics between virtual synchronous generator and droop control in inverter-based distributed generators," *IEEE Transactions on Power Electronics*, vol. 31, pp. 3600–3611, 2016.

[9] Q. Zhong and G. Weiss, "Synchronverters: Inverters that mimic synchronous generators," *IEEE Transactions on Industrial Electronics*, vol. 58, no. 4, pp. 1259–1267, 2011.

[10] X. Quan, R. Yu, X. Zhao, Y. Lei, T. Chen, C. Li, and A. Q. Huang, "Photovoltaic synchronous generator: Architecture and control strategy for a grid-forming pv energy system," *IEEE Journal of Emerging and Selected Topics in Power Electronics*, vol. 8, no. 2, pp. 936–948, 2020.

[11] J. Fang, H. Li, Y. Tang, and F. Blaabjerg, "On the inertia of future more-electronics power systems," *IEEE Journal of Emerging and Selected Topics in Power Electronics*, vol. 7, no. 4, pp. 2130–2146, 2019.

[12] B. I. Craciun, T. Kerekes, D. Sera, and R. Teodorescu, "Frequency support functions in large PV power plants with active power reserves," *IEEE Journal of Emerging and Selected Topics in Power Electronics*, vol. 2, no. 4, pp. 849–858, 2014.

[13] T. Hua, X. Yan, and W. Fan, "Research on power point tracking algorithm considered spinning reserve capacity in gird-connected photovoltaic system based on VSG control strategy," in *2017 IEEE 3rd International Future Energy Electronics Conference and ECCE Asia (IFEEC 2017 - ECCE Asia)*, 2017, pp. 2059–2063.

[14] X. Yan, J. Li, L. Wang, S. Zhao, T. Li, Z. Lv, and M. Wu, "Adaptive-MPPT-based control of improved photovoltaic virtual synchronous generators," *Energies*, vol. 11, no. 7, pp. 1–18, 2018.

[15] W. A. Omran, M. Kazerani, and M. M. A. Salama, "Investigation of methods for reduction of power fluctuations generated from large grid-connected photovoltaic systems," *IEEE Transactions on Energy Conversion*, vol. 26, no. 1, pp. 318–327, 2011.

[16] V. A. K. Pappu, B. Chowdhury, and R. Bhatt, "Implementing frequency regulation capability in a solar photovoltaic power plant," in *North American Power Symposium 2010*, 2010, pp. 1–6.

[17] H. Xin, Y. Liu, Z. Wang, D. Gan, and T. Yang, "A new frequency regulation strategy for photovoltaic systems without energy storage," *IEEE Transactions on Sustainable Energy*, vol. 4, no. 4, pp. 985–993, 2013.

[18] C. Zhong, Y. Zhou, and G. Yan, "A novel frequency regulation strategy for a pv system based on the curtailment power-current curve tracking algorithm," *IEEE Access*, vol. 8, pp. 77 701–77 715, 2020.

[19] A. Hoke and D. Maksimović, "Active power control of photovoltaic power systems," in *2013 1st IEEE Conference on Technologies for Sustainability (SusTech)*, 2013, pp. 70–77.

[20] Y. Yang, F. Blaabjerg, H. Wang, and M. G. Simões, "Power control flexibilities for grid-connected multi-functional photovoltaic inverters," *IET Renewable Power Generation*, vol. 10, no. 4, pp. 504–513, 2016.

[21] X. Li, H. Wen, Y. Zhu, L. Jiang, Y. Hu, and W. Xiao, "A novel sensorless photovoltaic power reserve control with simple real-time mpp estimation," *IEEE Transactions on Power Electronics*, vol. 34, no. 8, pp. 7521–7531, 2019.

[22] K. Yan, X. Wang, Y. Du, N. Jin, H. Huang, and H. Zhou, "Multi-step short-term power consumption forecasting with a hybrid deep learning strategy," *Energies*, vol. 11, no. 11, pp. 1–15, 2018.

[23] Y. Du, K. Yan, Z. Ren, and W. Xiao, "Designing localized mppt for pv system using fuzzy-weighted extreme learning machine," *Energies*, vol. 11, pp. 1–10, 2018.

[24] C. Zhang, Y. Du, X. Chen, and D. D. C. Lu, "Cloud motion tracking system using low-cost sky imager for PV power ramp-rate control," *Proceedings - 2018 IEEE International Conference on Industrial Electronics for Sustainable Energy Systems, IESES 2018*, vol. 2018-January, pp. 493–498, 2018.

[25] C. Zhang, Y. Du, X. Chen, and E. Lim, "Cloud motion forecasting and cloud base height estimation using two low-cost sky cameras," in *Energy Internet and Energy System Integration (EI2) 2018 2nd IEEE Conference*, 2018, pp. 1–6.

[26] K. Yan, Y. Du, and Z. Ren, "MPPT perturbation optimization of photovoltaic power system based on solar irradiance data classification," *IEEE Transactions on Sustainable Energy*, vol. 10, pp. 514–521, 2018.

[27] D. Yang, J. Kleissl, C. A. Gueymard, H. T. C. Pedro, and C. F. M. Coimbra, "History and trends in solar irradiance and PV power forecasting: A preliminary assessment and review using text mining," *Solar Energy*, vol. 168, pp. 60–101, 2018.

[28] H. Wen, Y. Du, X. Chen, E. Lim, H. Wen, L. Jiang, and W. Xiang, "Deep learning-based multi-step solar forecasting for pv ramp-rate control using sky images," *IEEE Transactions on Industrial Informatics*, pp. 1–1, 2020.

[29] X. Chen, Y. Du, and H. Wen, "Forecasting based power ramp-rate control for PV systems without energy storage," *2017 IEEE 3rd International Future Energy Electronics Conference and ECCE Asia, IFEEC - ECCE Asia 2017*, pp. 733–738, 2017.

[30] X. Chen, Y. Du, H. Wen, L. Jiang, and W. Xiao, "Forecasting-based power ramp-rate control strategies for utility-scale pv systems," *IEEE Transactions on Industrial Electronics*, vol. 66, no. 3, pp. 1862–1871, 2018.

[31] X. Chen, Y. Du, E. Lim, H. Wen, and L. Jiang, "Sensor network based pv power nowcasting with spatio-temporal preselection for grid-friendly control," *Applied Energy*, vol. 255, p. 113760, 2019.

[32] C. Meira, E. Vicente, and F. Tofoli, "Experimental evaluation of global maximum power point techniques under partial shading conditions," *Solar Energy*, vol. 196, pp. 49–73, 01 2020.

[33] Y. Han, N. Wang, M. Ma, H. Zhou, S. Dai, and H. Zhu, "A pv power interval forecasting based on seasonal model and nonparametric estimation algorithm," *Solar Energy*, vol. 184, pp. 515–526, 2019.

[34] D. Yang, Z. Dong, T. Reindl, P. Jirutitijaroen, and W. M. Walsh, "Solar irradiance forecasting using spatio-temporal empirical kriging and vector autoregressive models with parameter shrinkage," *Solar Energy*, vol. 103, pp. 550–562, 2014.

[35] C. Z. Ally, Y. Sun, and E. C. W. de Jong, "Impact of virtual inertia on increasing the hosting capacity of island diesel-pv ac-grid," in *2018 53rd International Universities Power Engineering Conference (UPEC)*, 2018, pp. 1–6.

[36] A. Hoke and D. Maksimović, "Active power control of photovoltaic power systems," in *2013 1st IEEE Conference on Technologies for Sustainability (SusTech)*, 2013, pp. 70–77.

[37] F. Belhachat and C. Larbes, "Comprehensive review on global maximum power point tracking techniques for pv systems subjected to partial shading conditions," *Solar Energy*, vol. 183, pp. 476 – 500, 2019.

[38] H. Zhou, Y. Zhang, L. Yang, Q. Liu, K. Yan, and Y. Du, "Short-term photovoltaic power forecasting based on long short term memory neural network and attention mechanism," *IEEE Access*, vol. 7, pp. 78 063–78 074, 2019.

[39] Z. Liu, L. Li, M. Tseng, and M. Lim, "Prediction short-term photovoltaic power using improved chicken swarm optimizer - extreme learning machine model," *Solar Energy*, vol. 248, p. 119272, 2020.

[40] H. Pedro, D. Larson, and C. Coimbra, "A comprehensive dataset for the accelerated development and benchmarking of solar forecasting methods," *Journal of Renewable and Sustainable Energy*, vol. 11, p. 036102, 05 2019.

[41] V. N. Lal and S. N. Singh, "Control and performance analysis of a single-stage utility-scale grid-connected pv system," *IEEE Systems Journal*, vol. 11, no. 3, pp. 1601–1611, 2017.

[42] A. Podder, N. Roy, and H. Pota, "Mppt methods for solar pv systems: A critical review based on tracking nature," *IET Renewable Power Generation*, vol. 13, 04 2019.

[43] P. Hasanpor Divshali and C. Evens, "Optimum operation of battery storage system in frequency containment reserves markets," *IEEE Transactions on Smart Grid*, vol. 11, no. 6, pp. 4906–4915, 2020.

[44] E. Cirés, J. Marcos, I. de la Parra, M. García, and L. Marroyo, "The potential of forecasting in reducing the lcoe in pv plants under ramp-rate restrictions," *Energy*, vol. 188, p. 116053, 2019.

[45] M. Obi, S. Jensen, J. B. Ferris, and R. B. Bass, "Calculation of levelized costs of electricity for various electrical energy storage systems," *Renewable and Sustainable Energy Reviews*, vol. 67, pp. 908–920, 2017.

[46] W. A. Omran, M. Kazerani, and M. M. A. Salama, "Investigation of methods for reduction of power fluctuations generated from large grid-connected photovoltaic systems," *IEEE Transactions on Energy Conversion*, vol. 26, no. 1, pp. 318–327, 2011.

Jiaming Chang received the B.S. degree in electrical engineering from Xi'an Jiaotong-Liverpool University, Suzhou, China, in 2016, and the M.S. degree in sustainable energy technology in 2018 from the University of Liverpool, Liverpool, U.K., where he is currently working toward the Ph.D. degree in electrical engineering.

His current research interests include solar power forecasting, photovoltaic power systems reliability, and micro-grid.

Yang Du (Senior Member, IEEE) received the Ph.D. degree in electrical engineering from The University of Sydney, Sydney, NSW, Australia, in 2013.

From 2013 to 2014, he was with the Masdar Institute of Science and Technology, Abu Dhabi, UAE, as a Postdoctoral Research Fellow. From 2014 to 2018, he was a Lecturer with Xi'an Jiaotong-Liverpool University, Suzhou, China, where he maintains an honorary position. He joined James Cook University, Cairns, QLD, Australia, in 2019. He was a Visiting Scientist with the Massachusetts Institute of Technology, Cambridge, MA, USA, in 2018. His research interest includes solar forecasting, renewable energy integration, power electronics and smart grid.

Dr. Du is currently an Associate Editor for IET Renewable Power Generation.

Eng Gee Lim (Senior Member, IEEE) received the BEng(Hons) and PhD degrees in Electrical and Electronic Engineering from the University of Northumbria, UK. Prof. Lim worked for Andrew Ltd, a leading communications systems company in the United Kingdom from 2002 to 2007. Since August 2007, Prof. Lim has been at Xian Jiaotong-Liverpool University, where he was formally the head of EEE department and University Dean of Research and Graduate studies. Now, he is School Dean of Advanced Technology, director of AI university research centre and also professor in department of Electrical and Electronic Engineering. He has published over 100 refereed international journals and conference papers.

His research interests are Artificial Intelligence, robotics, AI+ Health care, international Standard (ISO/IEC) in Robotics, antennas, RF/microwave engineering, EM measurements/simulations, energy harvesting, power/energy transfer, smart-grid communication; wireless communication networks for smart and green cities. He is a charter engineer and Fellow of IET. In addition, he is also a senior member of IEEE and Senior Fellow of HEA.

Huiqing Wen (Senior Member, IEEE) received his B.S. and M.S. degrees in Electrical Engineering from Zhejiang University, Hangzhou, China, in 2002 and 2006, respectively. In 2009, he received his Ph.D. in Electrical Engineering from the Chinese Academy of Sciences, Beijing, China.

From 2009 to 2010, he has been an electrical engineer working with the GE (China) Research and Development Center Company, Ltd., Shanghai, China. From 2010 to 2011, he was an engineer at the China Coal Research Institute, Beijing, China. From 2011 to 2012, he was a postdoctoral fellow at the Masdar Institute of Science and Technology, Abu Dhabi, United Arab Emirates. In 2013, he joined the Electrical and Electronic Engineering Department of Xi'an Jiaotong-Liverpool University (XJTLU), Suzhou, China. Currently, he is an associate professor at the XJTLU. He has published more than 50 peer reviewed technical papers in leading journals. His research interests include renewable energy, electric vehicle, power electronics, microgrid, and power semiconductor devices.

He is the Associate Editor of IEEE ACCESS, International Journal of Photoenergy, and Journal of Power Electronics.

Xingshuo Li (Member, IEEE) received the B.S. degree in computer science from Zhengzhou University, Zhengzhou, China, in 2012, and and the M.S. degree in sustainable energy technology with distinction from Xi'an Jiaotong-Liverpool University, Suzhou, China, in 2015. In 2019, he received the Ph.D degree from of Liverpool, Liverpool, U.K.

He is currently a Lecturer with School of Electrical and Automation Engineering, Nanjing Normal University, Nanjing, China. His research interest includes renewable energy technology and distributed generation, especially ancillary service, power forecasting and fault diagnosis in Photovoltaic systems.

Lin Jiang (Member, IEEE) received the B.S. and M.S. degrees in electrical engineering from the Huazhong University of Science and Technology (HUST), Wuhan, China, in 1992 and 1996, respectively, and the Ph.D. degree in electrical engineering from the University of Liverpool, Liverpool, U.K., in 2001. From 2001 to 2003, he was a Postdoctoral Research Assistant with the University of Liverpool, and from 2003 to 2005, a Postdoctoral Research Associate with the Department of Automatic Control and Systems Engineering, The University of Sheffield, Sheffield, U.K. From 2005 to 2007, he was a Senior Lecturer with the University of Glamorgam, Wales, U.K., and in 2007, he joined the University of Liverpool.

He is currently a Reader with the University of Liverpool. His current research interests include control and analysis of power system, smart grid, and renewable energy.